Bull. Mater. Sci., Vol. 39, No. 5, September 2016, pp. 1233–1243. © Indian Academy of Sciences.
DOI 10.1007/s12034-016-1243-6

Luminescence properties of ZnO/TiO_2 nanocomposite activated by Eu^{3+} and their spectroscopic analysis

PANKAJ KUMAR BAITHA and J MANAM*
Department of Applied Physics, Indian School of Mines, Dhanbad 826004, India

MS received 29 November 2015; accepted 9 March 2016

Abstract. **A new type of novel orange-red emitting Eu-doped ZnO/TiO_2 nanocomposite phosphors have been synthesized by simple low temperature co-precipitation route. Structure and morphology of the prepared sample have been investigated using X-ray diffraction and field emission scanning electron microscopy (FESEM) techniques. XRD pattern confirmed the presence of both phases of ZnO and TiO_2 simultaneously. The luminescence properties, such as photoluminescence (PL) excitation and emission spectra, Judd–Ofelt parameters, CIE colour coordinates and the dependence of luminescence intensity on the doping level were investigated. The luminescence spectrum characteristics of Eu^{3+} ions have a strong dependence on Eu^{3+} doping levels as well as ZnO/TiO_2 ratio variations. The photoluminescence results indicate that these phosphors could be efficiently excited by near-ultraviolet radiation, which causes emissions in orange–red regions.**

Keywords. **Nanocomposite; co-precipitation; enhanced luminescence; Judd–Ofelt parameters.**

1. Introduction

Lanthanide ions have long been used as an important dopant for the production of phosphor materials [1]. These rare earth ions produce intense and sharp emissions in visible range under UV excitation, when incorporated in an appropriate host matrix which is usually oxide materials [2]. These oxide materials are normally semiconductive in nature. Now-a-days, there are broad areas of applications such as luminescence, display devices [3,4], optoelectronic devices [3,4], sensing devices [5] etc., where the oxide material incorporated with lanthanide ions have been effectively and efficiently utilized. For the purpose of luminescence application, the primary need is a significant enhancement in emission intensity. Enhancement in luminescence can be achieved by energy transfer from encapsulated host matrix with the help of doping and co-doping of suitable lanthanide ions [6]. In the last few decades, such enhancement has achieved almost near to the theoretical limit and have very little room to work on that. Hence, a new type of host materials is required for the improvement of luminescence properties for opto-electronic applications [7]. In recent years, many efforts have been made for the enhancement of the luminescence intensity by using conventional route, but no significant outcome has been reported and therefore, to overcome this problem, researchers have to think about a new kind of material such as multifunctional hybrid material, composite material, etc. Soon after, researchers got a new hope in the form of nanocomposite-doped with suitable lanthanide ions for the improvement of luminescence behaviour [8,9]. Lanthanide-doped nanocomposite semiconductor is one of the promising host material for the required purpose as oxides show their unique behaviour in the form of nanocomposite. The coupling of two semiconductor nanoparticles with different band gap widths has been established in many studies as one of the most effective ways to slow the recombination of electron–hole pairs [10–13], which facilitate the enhancement of luminescence properties.

Among different semiconductor oxides, zinc oxide is one of the promising material due to their stable physical, chemical and thermal behaviours [14]. ZnO is well known for its luminescence behaviour as it gives broad green emission caused by defect states and ultraviolet emission through band edge transition [15]. To get better luminescence property, one may require incorporation of rare earth (RE) ions in the ZnO. But it is a difficult task due to large mismatch of ionic radii and charge imbalance of Zn^{2+} and RE^{3+}. On the other side, ZnO-based composite material doped with rare earth ions are easy to synthesize to get better emission properties. Nanoscale composite materials containing the binary system of zinc oxide and titanium oxide are interesting because of their potential applications in optoelectronic devices individually [16].

In this study of Eu^{3+}, TiO_2 and ZnO were chosen as activator ion host material and sensitizer [17]. The benefit of choosing this combination of materials is that it can produce all primary lights i.e., blue, green and red providing the facility for white light applications.

2. Experimental

Eu^{3+}-doped ZnO/TiO_2 nanocomposites were successfully prepared by simple co-precipitation method. Zinc sulfate, titanium oxysulfate and europium chloride were used as

*Author for correspondence (jairam.manam@gmail.com)

starting materials. To synthesize the required composite, appropriate amounts of these starting materials were dissolved in 50 ml of deionized water and stirred for a few minutes until the solution becomes transparent. An another solution of NaOH (2 mol% conc.) was also prepared. The aqueous solution of NaOH was added dropwise and stirred vigorously. With addition of NaOH solution, the pH value of the solution was adjusted to about 7. With the addition of NaOH in first solution, a large amount of white precipitate was formed. This white precipitate was filtered with Whatman-42 filter paper and washed several times with ethanol and deionized water until the unwanted ions, such as SO_4^{2-} and Cl^- are totally removed. After the filtration, the filtrate was kept in a hot air oven for 1.5 h at 80°C to make it dry. A fine powder was obtained after crushing with mortar and pestle. Finally, the powder was placed in a furnace for annealing process.

The synthesized powder was characterized for structural and optical properties. X-ray diffraction (XRD) spectra were recorded on Bruker D8 Focus in a wide range of Braggs angles, $20° \leq 2\theta \leq 80°$ with Cu target having $K\alpha = 1.5406$ Å with a scanning rate 2° per minute. The morphological studies as well as elemental composition were investigated by field emission scanning electron microscopy (FESEM) characterization on Supra 55 (Germany). Agilent Cary 5000 UV–Vis–NIR spectrophotometer has been used for UV–Vis diffuse reflectance studies on a wavelength range of 200–1200 nm. For photoluminescence (PL) studies, we used commercially available personal computer based Hitachi FL 2500 fluorescence spectrometer having 150 W xenon lamp. The PL emission spectra were taken in the wavelength range of 350–700 nm.

3. Results and discussion

3.1 *Structural and morphological studies*

The phase identification of the prepared sample was carried out by XRD on a wide range of Bragg angles $20° \leq 2\theta \leq 80°$ with Cu target having $K\alpha = 1.5406$ Å with a scanning rate 2° per minute. Figure 1 shows the XRD patterns of samples annealed at three different temperatures (400, 600 and 800°C). XRD patterns are compared with standard JCPDS data and it is found that it is well matched with PDF nos 83-2243 (TiO_2) and 75-1533 (ZnO). From figure 1, one can clearly identify both the phases of ZnO and TiO_2 which confirm the formation of the desired compound. Apart from that, some unidentified peaks with very small intensity was also observed, which is possibly due to impurity of sample mainly caused by unreacted components from the synthesis process or may be intermediate compounds. The main characteristic diffraction peaks of TiO_2 and ZnO were found at 25.80 and 35.86°, which shows a very slight shift to the higher angle side compared to corresponding JCPDS file no., which is possibly due to the incorporation of Eu^{3+} ions in the host lattice and due to that lattice atoms get displaced and redistribution of density of states in the unit cell occur. The shifting in characteristic peaks causes the decrease in lattice parameter [18] compared to respective

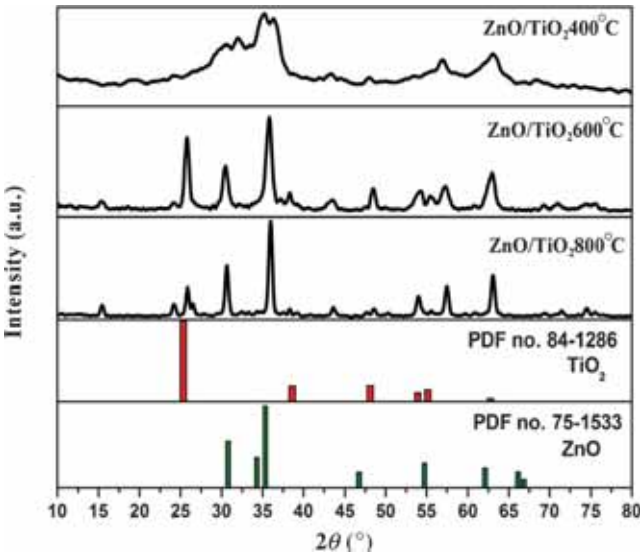

Figure 1. X-ray diffraction patterns of Eu^{3+}-doped ZnO/TiO_2 nanocomposite for different annealing temperatures.

JCPDS file. This is because of mismatch of ionic radii of Eu^{3+} and Zn^{2+}/Ti^{4+} ions. XRD pattern also suggests that for the desired nanocomposite, low annealing temperature is suitable because at higher temperature, it starts reacting with each other, causing the formation of intermediate compound, the same is observed in our case for the highest annealing temperature (800°C). The XRD profile also revealed that the annealing temperature plays an important role in the crystallinity of the sample. At lower annealing temperature (400°C), XRD pattern shows broader peaks, whereas at higher annealing temperature, peaks become sharper which indicates improvement in the crystallinity of the samples. The crystallite sizes of the synthesized powder were calculated using Debye Sherrer formula is given by

$$D = 0.9\lambda/\beta \cos\theta,$$

where D is the crystallite size, λ the wavelength of X-ray and β the full-width at half-maximum (FWHM) and by using this formula the crystallite size is estimated by considering the main characteristic peaks of XRD, which is found in the range of 15–30 nm. In another approach, Hall–Williamson relation was also used to calculate the exact crystallite size is given by

$$\frac{\beta \cos\theta}{\lambda} = \frac{1}{D} + \frac{\varepsilon \sin\theta}{\lambda},$$

where ε is the microstrain present in the sample. Figure 2 shows the Hall–Williamson plot of the XRD graph for ZnO/TiO_2 composite annealed at different temperatures. It shows that for annealing temperature of 400°C, crystallite size is 30.58 nm and for annealing temperature of 600°C, it is 38.16 nm, whereas for annealing temperature of 800°C, crystallite size is 24.87 nm. It can be understood that at a lower annealing temperature, the sample is agglomerated in nature, hence, crystallite size is large and as the annealing temperature increases up to 600°C, crystallite gets complete

growth and as a result of smaller size but for further increasing the annealing temperature causes the reaction between ZnO and TiO_2 to form intermediate compound and results in decrease in crystallite size.

Figure 3 shows the FESEM images of Eu^{3+}-doped ZnO/TiO_2 nanocomposite samples annealed at different annealing temperatures as well as with different compositions. All samples exhibit irregular grain type structures which are agglomerated in morphology. As the annealing temperature increases, these agglomeration reduces and starts to form a more crystalline type structure. In the as-prepared sample, the sizes of most of the grains are in the range of 20–25 nm and as the annealing temperature increases, the grain size is found in the ranges of 20–30, 30–35 and 40–60 nm for annealing temperatures of 400, 600 and 800°C, respectively. From the images, it was found that in all samples, the particles are almost uniformly distributed throughout the surface which is possibly due to homogeneous distribution of temperature during the synthesis of material as it is prepared at room temperature.

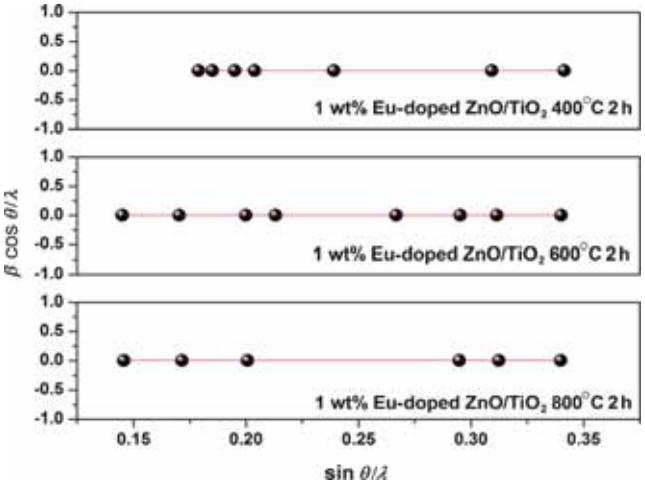

Figure 2. Hall–Williamson plot of Eu^{3+}-doped ZnO/TiO_2 nanocomposite for different annealing temperatures.

3.2 *Optical studies*

3.2a *UV–Vis study*: The diffuse reflectance spectra of Eu^{3+}-doped ZnO/TiO_2 nanocomposite are carried out on the prepared sample for different compositions of ZnO and TiO_2 as well as different doping concentrations of Eu^{3+} for calculation of the optical band gap. The diffuse reflectance spectra were recorded at room temperature in the range of 200–800 nm wavelengths as shown in figure 4. In the reflectance spectra, a sharp band was observed near 320 nm as absorption edge. This represents that this absorption of wavelength 320 nm by the sample relates to band gap of the material. Related to absorption edge, one interesting phenomenon is observed with ZnO variation. With increasing the ZnO content in the material, a blue shift is observed in absorption edge. This may be ascribed either to reduction in particle size with increasing ZnO concentration or to 'Burstein–Moss effect' [19,20], according to which the increase in the Fermi level in the conduction band of a degenerate semiconductor lead to energy band-widening, caused by the effect of increasing carrier concentration. Keeping the consistency with photoluminescence excitation spectra, the absorption band related to $^7F_0 \rightarrow {}^5D_2$ and $^7F_0 \rightarrow {}^5D_1$ transitions of Eu^{3+} ions are also monitored at 465 and 532 nm, respectively. The presence of these bands confirms the existence of metastable energy state due to Eu^{3+} between valence and conduction band.

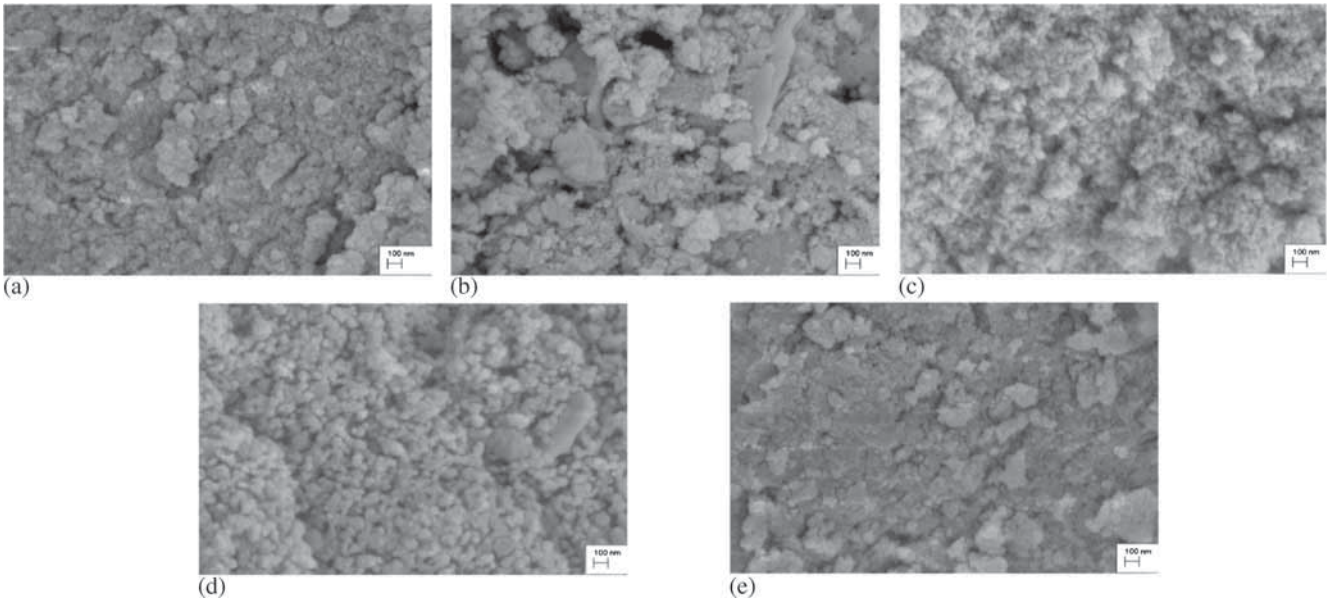

Figure 3. FESEM images of 1 wt% Eu-doped ZnO/TiO_2 (molar ratio = 50:50) at annealing temperatures of (**a**) as prepared, (**b**) 400°C, (**c**) 600°C, (**d**) 800°C and (**e**) 1.5 wt% Eu-doped ZnO/TiO_2 (molar ratio = 40:60).

3.2b *Band gap calculation*: The diffuse reflectance spectra of Eu^{3+}-doped ZnO/TiO_2 nanocomposite are used to calculate the estimated band gap (E_g) of the synthesized powder sample with the help of Kubelka–Munk theory. In diffuse reflectance spectra, the ratio of light reflected from the sample to an ideal nonabsorbing reference sample (which is $BaSO_4$ in our case) are measured as a function of wavelength. Using the Kubelka–Munk relation [21], reflectance (R_α) is converted to Kubelka–Munk ($F(R_\alpha)$) function which is given by

$$F(R_\alpha) = \frac{(1 - R_\alpha)^2}{2R_\alpha}.$$

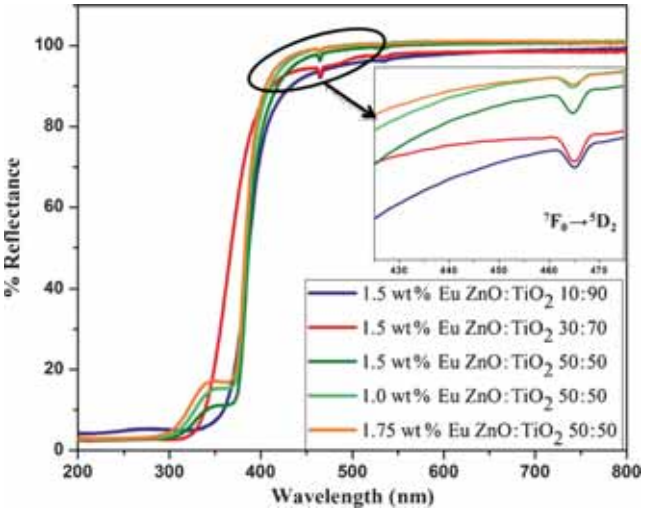

Figure 4. Diffuse reflectance spectrum of Eu^{3+}-doped ZnO/TiO_2 nanocomposite for different concentrations of Eu and different molar ratios of ZnO and TiO_2.

The Kubelka–Munk function is a function equivalent to absorption co-efficient (α). The band gap energy of a material is related to absorption coefficient, α through a well-known Tauc relation is given by

$$\alpha h\nu = C(h\nu - E_g)^n,$$

where $n = 1/2$ for direct bandgap and 2 for indirect bandgap. Thus, the bandgap of the material is determined by plotting $[F(R_\alpha)h\nu]^{1/n}$ against photon energy $h\nu$, the value of E_g was obtained by extrapolating the linear fitted regions to $[F(R_\alpha)h\nu]^{1/n} = 0$, as shown in figure 5. Since the prepared material is a composite of ZnO/TiO_2-doped with Eu in which ZnO is a direct bandgap material, where TiO_2 is an indirect bandgap material, hence, calculation of band gap was done for both the conditions i.e., direct and indirect bandgaps and it was found that the sample having low ZnO concentration (for 10 and 30 mole%) shows best fitting in indirect bandgap calculation and was found to be 3.15 and 3.37 eV. This is because of the presence of TiO_2 as major component in the sample which is an indirect bandgap material. As the concentration of ZnO become equivalent to TiO_2, the best fitting is found for direct bandgap condition and the value of bandgap was found to be 3.8 eV. Thus, the variation of ZnO content in the material causes the modification in band gap. With increasing the ZnO content, band gap increases from 3.15 to 3.8 eV. This indicates that tuning in band gap is possible with the variation of ZnO in the Eu^{3+}-doped ZnO/TiO_2 nanocomposite. Another interesting thing which was observed is small amounts of Eu^{3+} doping does not affect too much, but for higher doping, band gap increases from 3.8 to 3.9 eV in ZnO/TiO_2 (50 : 50). The insertion of lattice disorder caused by incorporation of Eu^{3+} and the presence of ZnO may be the possible reason for the variation of band gap [22].

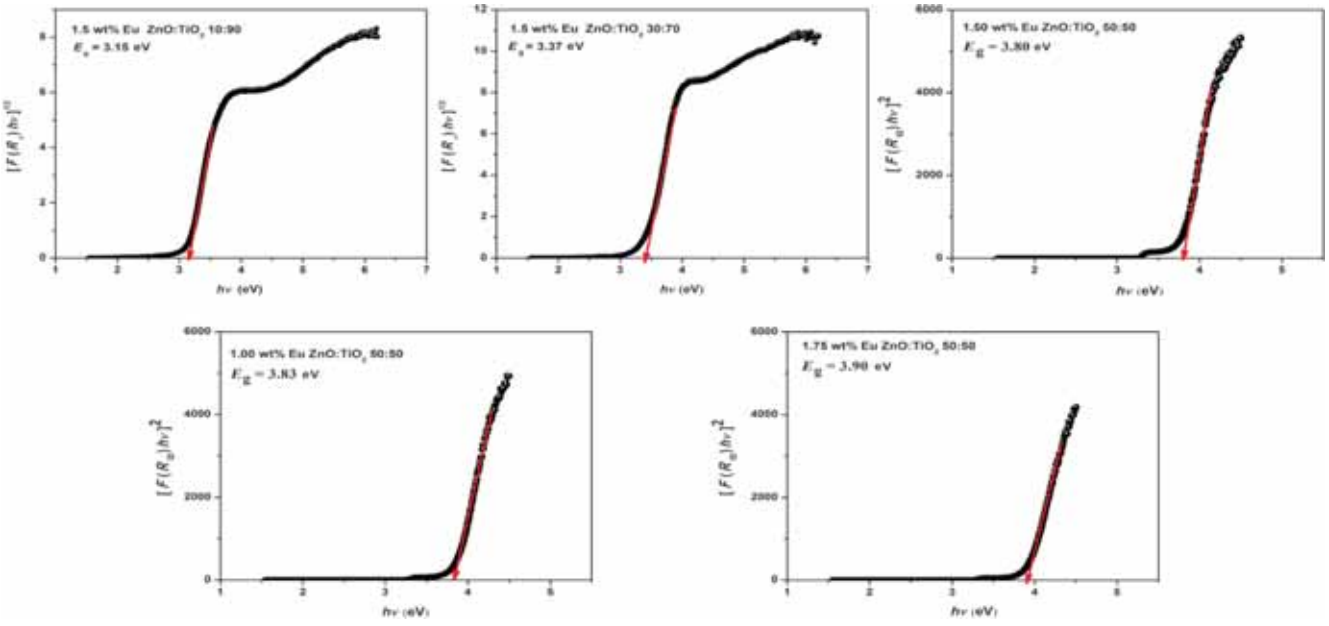

Figure 5. Kubelka–Munk treatment of reflectance spectrum to calculate the band gap of Eu^{3+}-doped ZnO/TiO_2 nanocomposite for different concentrations of Eu and different molar ratios of ZnO and TiO_2.

3.2c *Luminescence study: Effect of annealing*: Room temperature PL emission spectra for 393 nm excitation of 1 wt% Eu^{3+}-doped ZnO/TiO_2 nanocomposite samples annealed at different temperatures are shown in figure 6. The figure shows two strong emission peaks centred at 595 and 619 nm with some weak emissions peaks at different centres, which is the characteristic emission of Eu^{3+} ion from $^5D_0$ to $^7F_j (j = 0, 1, 2, 3, 4, 5, 6)$. It is important to note that the fluorescence intensity ratio, I of $^5D_0 \rightarrow {}^7F_2$ to $^5D_0 \rightarrow {}^7F_1$ transition changes with change in annealing temperature [23]. It is well known that the transition $^5D_0 \rightarrow {}^7F_2$ is an electric dipolar transition and is very sensitive to ligand field and thus, a larger probability has been postulated for this transition because of decrease in symmetry and increase in covalency. On the other hand, the emission peak centred at 595 nm for $^5D_0 \rightarrow {}^7F_1$ transition is due to magnetic dipole transition hardly affected by crystal field around Eu^{3+} ion in matrix. Hence, I is the intensity ratio of transition from $^5D_0 \rightarrow {}^7F_2$ to $^5D_0 \rightarrow {}^7F_1$, which provide a measure of degree of distortion using inversion symmetry of local environment of Eu^{3+} ions. In the present case, the calculated fluorescence intensity ratio was found to be 2.36, 2.71, 3.74 and 3.34 for as prepared and annealed samples for 2 h at 400, 600 and 800°C, respectively. This trend represents the increase in fluorescence intensity ratio with annealing temperature, suggesting the change in symmetry site occupied by Eu^{3+} ions which may be related to the some surface defects which possibly affects the crystal structure. These surface defects are the possible reason for increase in degree of disorder and decrease in local symmetry of Eu^{3+} ions located at the surface of the particle [24]. Owing to lowering the local symmetry of Eu^{3+} ions, the probability of $^5D_0 \rightarrow {}^7F_2$ transition increases and hence, enhance the red emission over orange emission although the luminescence spectra are still mixture of orange and red emission.

Effect of doping concentration on PL: PL performance of a material can be improved with the help of changing the doping concentration. The variation in dopant concentration is very important to get the optimized concentration of dopant for best PL performance. PL emission spectra for ZnO/TiO_2 nanocomposite doped with Eu^{3+} ions for different doping concentrations (0.50, 0.75, 1.00, 1.25, 1.50, 1.75 and 2.00 wt%) are shown in figure 7 at excitation wavelength 393 nm annealed at 400°C and it was found that PL intensity is maximum for 1.50 wt% of Eu^{3+} doping. From the PL emission of Eu^{3+}-doped ZnO/TiO_2 nanocomposite, it was found that the emission spectra contain different narrow peaks centred at 538, 557, 581, 594, 617, 656 and 702 nm. These peaks assigned to $^5D_1 \rightarrow {}^7F_1$, $^5D_1 \rightarrow {}^7F_2$, $^5D_0 \rightarrow {}^7F_0$, $^5D_0 \rightarrow {}^7F_1$, $^5D_0 \rightarrow {}^7F_2$, $^5D_0 \rightarrow {}^7F_3$ and $^5D_0 \rightarrow {}^7F_4$ transitions of the $4f^6$ configuration of Eu^{3+} ions, respectively [25,26]. Among these, two most intense emissions correspond to magnetic and electric dipole transitions. The electric dipole transition is observed at 617 nm due to $^5D_0 \rightarrow {}^7F_2$ transition which is more intense than magnetic dipole transition observed at 594 nm due to $^5D_0 \rightarrow {}^7F_1$ transition. The most intense red emission is mainly attributed to the larger degree of disorder and lower local symmetry or noncentrosymmetric without inversion centre of Eu^{3+} ions.

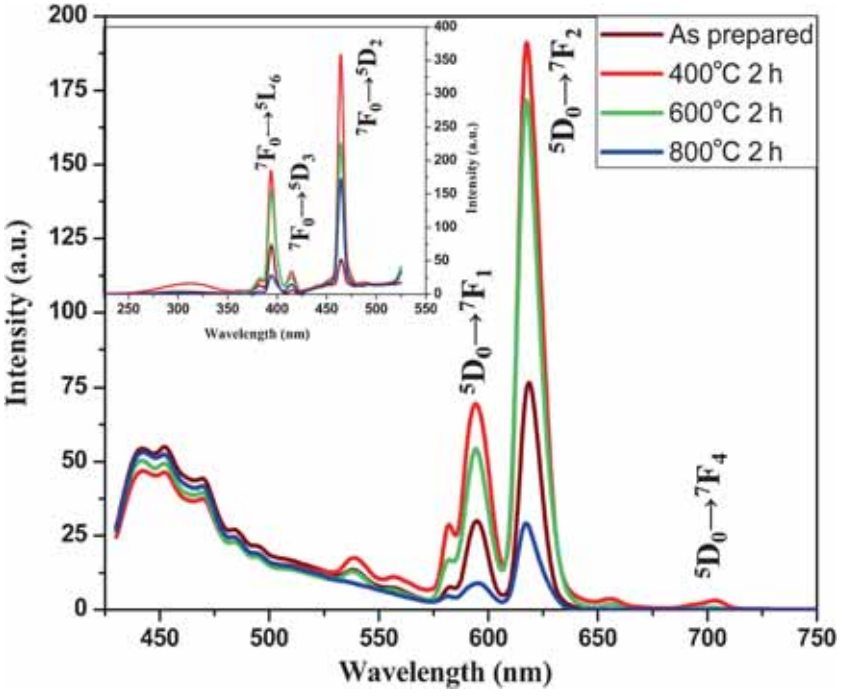

Figure 6. Photoluminescence emission spectra of 1 wt% Eu^{3+}-doped ZnO/TiO_2 nanocomposite for different annealing temperatures excited by 393 nm wavelength. Inset shows excitation spectra for same samples monitoring the emission wavelength of 617 nm.

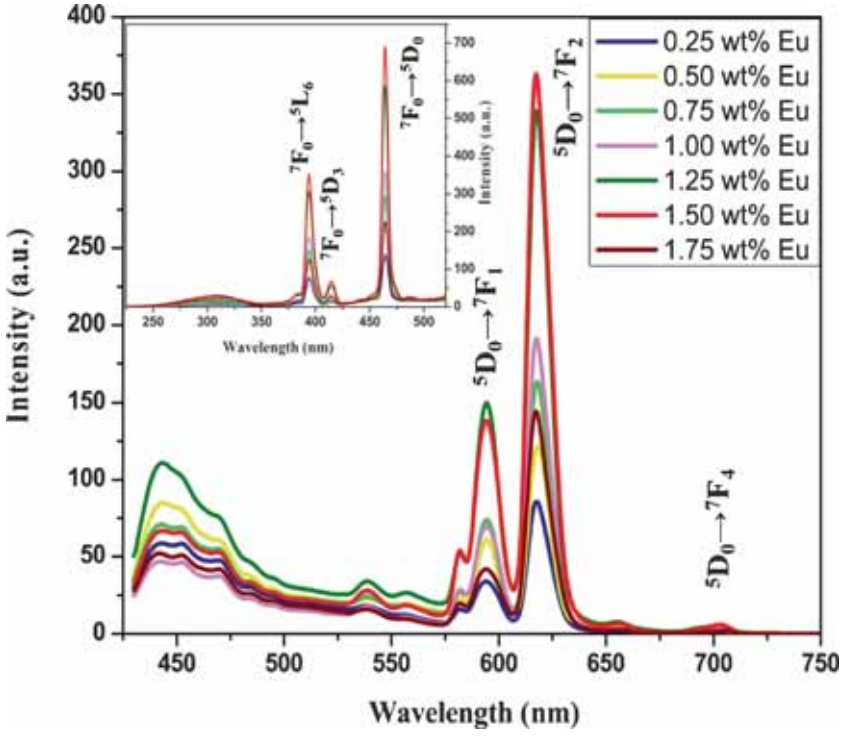

Figure 7. Photoluminescence emission spectra of Eu^{3+}-doped ZnO/TiO_2 nanocomposite for different concentrations of Eu^{3+} excited by 393 nm wavelength. Inset shows excitation spectra for same samples monitoring the emission wavelength of 617 nm.

Actually, incorporation of dopant with larger ionic radii than the doping site (which is in our case both may be possible Zn^{2+} as well as Ti^{4+}) causes the local distortion in the host lattice [27]. On the other side, it is well known fact that the orange emission centred at 594 nm is due to magnetic dipole transition which is allowed only if Eu^{3+} ions occupy a site with inversion symmetry or low centrosymmetric site. The presence of both electric and magnetic dipole transitions and dominated by the electric dipole transition indicates that Eu^{3+} ions not only occupy the site with inversion symmetry, but some Eu^{3+} ions also occupy the site without inversion symmetry.

Eu^{3+}–Eu^{3+} energy transfer and concentration quenching: The nonradiative transition is a phenomenon which causes the decrease in luminescence which generally occurs due to exchange interaction, radiation reabsorption, or a multipole–multipole interaction [28,29]. In a typical case, as the doping concentration increases, the effective distance between Eu^{3+} ions decreases and as a result PL intensity increases. With increasing the dopant concentration, a condition is found where PL intensity is maximum for a particular doping concentration and beyond that limit, a condition is met where distance between two neighbour Eu^{3+} ions is such that Eu^{3+} ions starts interacting with each other resulting in the increase of nonradiative relaxation and hence, PL intensity decreases. To understand such type of phenomenon, it is necessary to find out the critical distance (R_c) between two neighbour Eu^{3+} ions. To find out this critical distance, we used Blasse formula [30,31] which is

$$R_c \approx 2\left[\frac{3V}{4\pi CN}\right]^{1/3},$$

where C is the critical concentration of the dopant, N the number of Ti ions in the unit cell and V the volume of the unit cell. In our case, $N = 4$, $C = 0.02$ and $V = 136.31$ Å^3 and we found that the value of R_c is 21.58 Å. It is known that if the value of R_c is greater than 5 Å, then exchange interaction [32] is no more effective and multipole–multipole interaction becomes important. Since the R_c value was calculated as 21.58 Å, the effective mechanism of concentration quenching was related to multipolar interaction.

Influence of the presence of ZnO in the composite: The effect of presence of ZnO on the emission intensity have been analysed by varying ZnO concentrations of 10, 20, 30, 40 and 50 mol% and it was observed that emission intensity enhanced with addition of ZnO in the host. 40 mol% of ZnO was found to be optimum concentration, for which emission intensity is maximum. The proper effect on the emission intensity for varying ZnO concentrations is shown in figure 8. This enhancement in the emission intensity may be ascribed to several reasons. Yadav *et al* [33] suggested that this enhancement is caused due to addition of ZnO in the sample

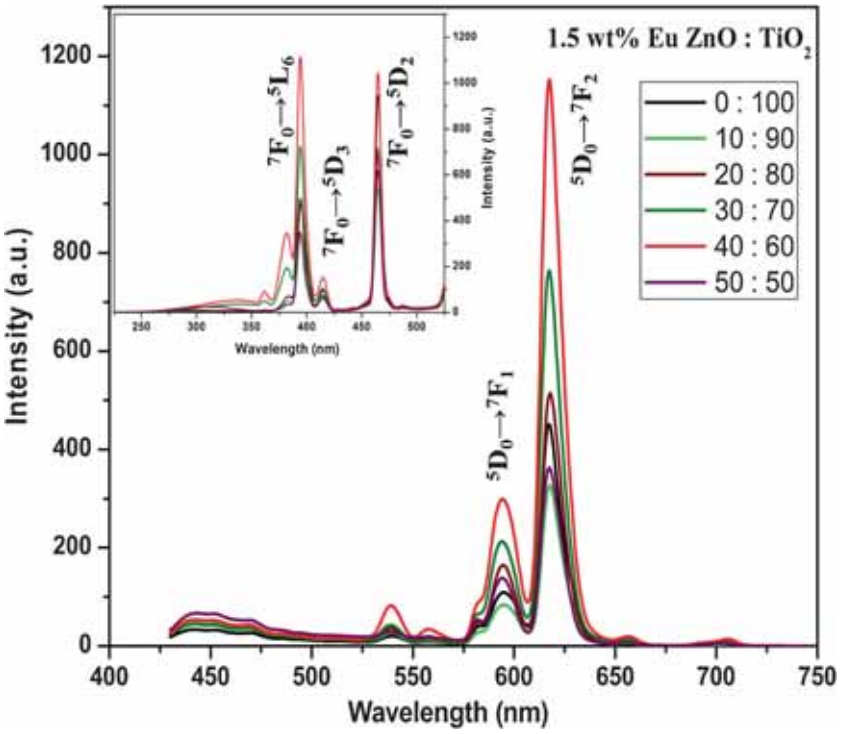

Figure 8. Photoluminescence emission spectra of 1.5 wt% Eu^{3+}-doped ZnO/TiO_2 nanocomposite for different molar ratios of ZnO and TiO_2 excited by 393 nm wavelength. Inset shows excitation spectra for same samples monitoring the emission wavelength of 617 nm.

which forms composite with TiO_2 and causes the decrease in nonradiative relaxation. This nonradiative relaxation is an important key which play a vital role in the emission intensity. The decrease in nonradiative relaxation causes the enhancement in emission intensity. Another possible reason for this enhancement is the presence of ZnO which occupies the remaining quenching site, and as a result, the space vacant in the lattice is occupied by ZnO which actually removes the unwanted impurities such as OH present in the host [34,35]. One may also ascribe this enhancement to the increase in crystallinity of the host material due to the presence of ZnO.

Excitation mechanism: The room temperature PL excitation spectra of ZnO/TiO_2 nanocomposite doped with Eu^{3+} ions were recorded in a wavelength range of 220–550 nm, keeping the emission wave length fixed at 617 nm and is shown in figures 6, 7 and 8. Normally, excitation spectra of phosphor having europium doping show two major parts: (i) charge-transfer state (CST) and (ii) intra-4f transition. Generally, the broad band centred at nearly 235 nm is due to transfer of electron to vacant 4f orbital of Eu^{3+} from 2p orbital of oxygen which may be ascribed as ligand-to-Eu^{3+} (metal) charge-transfer transitions (LMCT) [36]. According to Jorgensen, the position of charge transfer band can be estimated by using the formula

$$\sigma = [x_{\text{opt}}(X) - x_{\text{uncorr}}(M)]\,30 \times 10^3\ \text{cm}^{-1},$$

where σ represents the energy of charge transfer band, x_{opt} (X) is the optical electronegativity of the ligand anion, which is approximately the Pauling's electronegativity and x_{uncorr} (M) is the optical electronegativity of the central metal ion. The estimated energy for O2p → Eu4f CT band was found about 42600 cm^{-1}, which is equivalent to 235 nm. But in our case, we have not observed such type of Eu^{3+}–O^{2-} CT band, which is a very unique behaviour shown by the samples because generally, Eu^{3+} doped phosphor always show an excitation peak at 250 nm [37]. This phenomenon can be understood as weak covalency between Eu^{3+} and O^{2-} in the nanocomposite crystallite [38]. Apart from this, a broad excitation peak with very low intensity was found near 310 nm, corresponds to the host lattice absorbtion. Another part of excitation spectrum i.e., intra-4f transition show four sharp transitions in between 360–550 nm range. These peaks are very narrow and are observed due to direct excitation of Eu^{3+} ions from ground state ($^7F_0$) to higher excited states of 4f-manifold, such as $^5G_4$ (383 nm), $^5L_6$ (393 nm), $^5D_3$ (414 nm), $^5D_2$ (464 nm) and $^5D_1$ (533 nm), respectively. The more intense the excitation band is, the more effectively phosphors absorb the excited energy. Among these excitation transitions, $^7F_0$ → $^5D_2$ (464 nm) is the most intense one, which matches well with the commercially available blue GaN-based LED chips.

Evaluation of colour coordinates: The assessment and quantification of colour emitted by a substance is referred to as colorimetry or the 'science of colour'. Colorimetry

is the property which is directly associated with human eye. Actually, human eyes have property that when two or more colours are mixed together, it is visualized as single colour and the eye is unable to recognize the original dichromatic composition of that colour. A mathematical function called the colour matching function gives the resultant vision of eye when two or more colours are mixed together and it is represented by the CIE chromaticity diagram [39,40]. The CIE parameter of our samples are calculated using the GoCIE software and it was found that for lower concentration of Eu^{3+} doping, it emits pink colour due to the mixing of blue emission by host and red emission by Eu^{3+} and as the doping concentration increases, it shifted towards red region and also with increasing the ZnO content, the coordinate shifted more towards red region and get maximum red for 40% ZnO content. Figure 9 shows the pattern of shifting from blue–pink to orange–red region. Hence, wide colour tunability from blue–pink to orange–red is obtained in this Eu-doped ZnO/TiO_2 nanocomposite. The calculated CIE coordinates for different doping concentrations of Eu^{3+} and diffrent ratios of ZnO and TiO_2 are summerized in table 1.

Radiative properties: The spectral properties or radiative properties such as transition probability (A), total transition probability (A_T), radiative lifetime (τ_{rad}) and branching ratio (β_{rad}) of RE ions in the host can be calculated using a parameter called Judd–Ofelt parameters Ω_J ($J = 2,4,6$) [41,42]. Usually, the Judd–Ofelt intensity parameters are obtained from the absorption spectra, but in the case of Eu^{3+} doping, it is difficult to obtain J–O parameter because observable transition is not enough. However, the pure magnetic dipole transition $^5D_0 \rightarrow {}^7F_1$ allows the determination of the intensity parameters from the emission spectra. According to J–O theory, the magnetic dipole transition $^5D_0 \rightarrow {}^7F_1$ is independent of host environment. This can be used as a reference and hence, rate of magnetic dipole transition is represented by the equation [43,44]

$$A_{0\rightarrow 1} = \frac{64\pi^4 e^2 (\nu_{0\rightarrow 1})^3}{3h(2J+1)} n^3 S_{md} \quad \text{(magnetic dipole transition)}. \tag{1}$$

In the above equation, e is the charge of electron, n the refractive index, ν the wavenumber, h the Plank's constant, $2J + 1$ the degeneracy of the initial state and S_{md} the magnetic dipole transition line strength. S_{md} is independent from the host and have the value equal to 7.83×10^{-42} (dimensionless). The rate of magnetic dipole transition $A_{0\rightarrow 1}$ has the value $\approx 50\,cm^{-1}$ [44]. Similarly, the rate of electric dipole transition

Table 1. Calculated CIE coordinates for different doping concentrations of Eu^{3+} and different ratios of ZnO and TiO_2.

Sample	CIE (x,y) coordinates	
	x-coordinate	y-coordinate
0.25 wt% Eu-doped ZnO : TiO_2 (50:50)	0.30	0.23
0.50 wt% Eu-doped ZnO : TiO_2 (50:50)	0.31	0.23
0.75 wt% Eu-doped ZnO : TiO_2 (50:50)	0.35	0.25
1.00 wt% Eu-doped ZnO : TiO_2 (50:50)	0.41	0.27
1.25 wt% Eu-doped ZnO : TiO_2 (50:50)	0.39	0.26
1.50 wt% Eu-doped ZnO : TiO_2 (50:50)	0.44	0.29
1.75 wt% Eu-doped ZnO : TiO_2 (50:50)	0.36	0.24
2.00 wt% Eu-doped ZnO : TiO_2 (50:50)	0.43	0.29
1.50 wt% Eu-doped ZnO : TiO_2 (40:60)	0.56	0.33
1.50 wt% Eu-doped ZnO : TiO_2 (30:70)	0.55	0.32
1.50 wt% Eu-doped ZnO : TiO_2 (20:80)	0.52	0.31
1.50 wt% Eu-doped ZnO : TiO_2 (10:90)	0.46	0.28
1.50 wt% Eu-doped ZnO : TiO_2 (10:90)	0.44	0.29

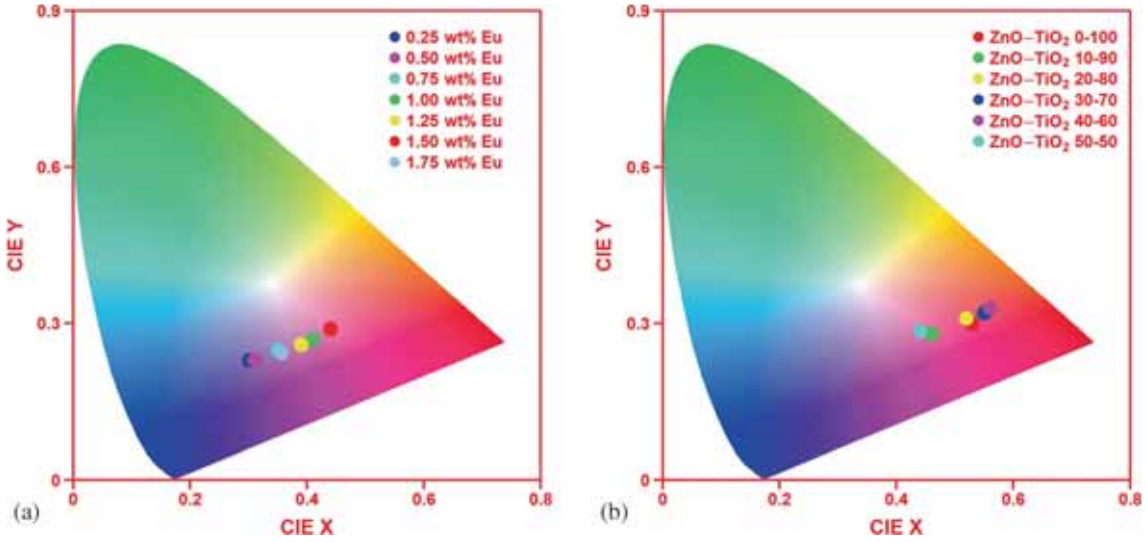

Figure 9. CIE chromaticity diagram for (**a**) different doping concentrations of Eu^{3+}-doped ZnO/TiO_2 nanocomposite and (**b**) different molar ratios of ZnO and TiO_2 doped with 1.5 wt% Eu^{3+}.

Table 2. J–O spectral parameter of ZnO/TiO$_2$:Eu^{3+}.

Sample	J–O intensity parameter Ω_2 (pm^2)	J–O intensity parameter Ω_4 (pm^2)	Transition	A_{0-1} (s^{-1})	$A_{0-2,4}$ (s^{-1})	A_τ (s^{-1})	τ_{rad} (ms)	β (%)	σ (λ_p) ($\times 10^{-21}$) cm^2	Asymmetry ratio
0.25 wt% Eu-doped	20.490	0.977	$^5D_0 \rightarrow {}^7F_1$	50	...	185.360	5.394	26.97	2.106	2.53
ZnO:TiO$_2$			$^5D_0 \rightarrow {}^7F_2$	...	132.265			71.35	6.491	
(50:50)			$^5D_0 \rightarrow {}^7F_4$	...	3.095			1.67	0.223	
0.50 wt% Eu-doped	17.643	1.067	$^5D_0 \rightarrow {}^7F_1$	50	...	167.267	5.978	29.89	2.379	2.18
ZnO:TiO$_2$			$^5D_0 \rightarrow {}^7F_2$	...	113.885			68.08	5.851	
(50:50)			$^5D_0 \rightarrow {}^7F_4$	...	3.381			2.02	0.209	
0.75 wt% Eu-doped	18.590	0.964	$^5D_0 \rightarrow {}^7F_1$	50	...	173.055	5.778	28.89	2.154	2.30
ZnO:TiO$_2$			$^5D_0 \rightarrow {}^7F_2$	...	120.001			69.34	5.843	
(50:50)			$^5D_0 \rightarrow {}^7F_4$	...	3.053			1.76	0.193	
1.00 wt% Eu-doped	20.567	0.925	$^5D_0 \rightarrow {}^7F_1$	50	...	185.690	5.385	26.92	1.788	2.54
ZnO:TiO$_2$			$^5D_0 \rightarrow {}^7F_2$	...	132.759			71.49	6.066	
(50:50)			$^5D_0 \rightarrow {}^7F_4$	...	2.931			1.57	0.185	
1.25 wt% Eu-doped	18.539	0.932	$^5D_0 \rightarrow {}^7F_1$	50		172.625	5.792	28.96	2.014	2.29
ZnO:TiO$_2$			$^5D_0 \rightarrow {}^7F_2$	...	119.6715			69.32	5.630	
(50:50)			$^5D_0 \rightarrow {}^7F_4$	...	2.953			1.71	0.182	
1.50 wt% Eu-doped	19.881	0.903	$^5D_0 \rightarrow {}^7F_1$	50	...	181.195	5.518	27.59	1.813	2.46
ZnO:TiO$_2$			$^5D_0 \rightarrow {}^7F_2$	...	128.334			70.82	5.843	
(50:50)			$^5D_0 \rightarrow {}^7F_4$	...	2.861			1.57	0.182	
1.75 wt% Eu-doped	26.481	1.172	$^5D_0 \rightarrow {}^7F_1$	50	...	224.648	4.451	22.25	1.814	3.28
ZnO:TiO$_2$			$^5D_0 \rightarrow {}^7F_2$	...	170.936			76.09	7.723	
(50:50)			$^5D_0 \rightarrow {}^7F_4$	...	3.712			1.65	0.209	
2.00 wt% Eu-doped	18.852	0.961	$^5D_0 \rightarrow {}^7F_1$	50	...	174.638	5.722	28.61	2.094	2.33
ZnO:TiO$_2$			$^5D_0 \rightarrow {}^7F_2$	...	121.693			69.64	7.723	
(50:50)			$^5D_0 \rightarrow {}^7F_4$	...	3.045			1.74	0.165	
1.50 wt% Eu-doped	26.158	0.950	$^5D_0 \rightarrow {}^7F_1$	50	...	221.860	4.170	22.53	1.554	3.24
ZnO:TiO$_2$			$^5D_0 \rightarrow {}^7F_2$	...	168.849			76.10	7.374	
(40:60)			$^5D_0 \rightarrow {}^7F_4$	...	3.011			1.35	0.167	
1.50 wt% Eu-doped	24.853	0.104	$^5D_0 \rightarrow {}^7F_1$	50	...	213.746	4.924	23.39	1.605	3.07
ZnO:TiO$_2$			$^5D_0 \rightarrow {}^7F_2$	...	160.426			75.05	7.021	
(30:70)			$^5D_0 \rightarrow {}^7F_4$	...	3.320			1.55	0.179	
1.50 wt% Eu-doped	23.229	0.982	$^5D_0 \rightarrow {}^7F_1$	50	...	203.054	4.678	24.62	1.758	2.87
ZnO:TiO$_2$			$^5D_0 \rightarrow {}^7F_2$	...	149.942			73.84	6.632	
(20:80)			$^5D_0 \rightarrow {}^7F_4$	...	3.112			1.53	0.162	
1.50 wt% Eu-doped	28.835	0.115	$^5D_0 \rightarrow {}^7F_1$	50	...	239.782	4.507	20.85	1.779	3.57
ZnO:TiO$_2$			$^5D_0 \rightarrow {}^7F_2$	...	186.129			77.62	8.376	
(10:90)			$^5D_0 \rightarrow {}^7F_4$	...	3.652			1.52	0.195	
1.50 wt% Eu-doped	34.802	0.152	$^5D_0 \rightarrow {}^7F_1$	50	...	279.462	3.578	17.89	1.689	4.31
ZnO:TiO$_2$			$^5D_0 \rightarrow {}^7F_2$	...	224.644			80.38	9.237	
(0:100)			$^5D_0 \rightarrow {}^7F_4$	...	4.817			1.72	0.150	

$A_{0\to J}$ of $^5D_0 \to {}^7F_{J=2,4,6}$ can be calculated using the formula [44,45]

$$A_{0\to J} = \frac{64\pi^4 e^2(\nu_{0\to 2,4})^3}{3hc^3}\frac{1}{4\pi\varepsilon_0}\chi \times \sum_{J=2,4,6}\Omega_J\left\langle {}^5D_0\right| U^{(J)} \left|{}^5F_{2,4,6}\right\rangle^2 \quad \text{(electric dipole transition)}, \tag{2}$$

where χ is a correction factor called Lorentz local field correction can be calculated by the relation given by $\chi = n(n^2+2)^2/9$ using refractive index of the host material. $\left\langle {}^5D_0\right| U^{(J)} \left|{}^5F_{2,4,6}\right\rangle^2$ is the squared reduced matrix element whose value is independent of the chemical environment of Eu^{3+} and the value of matrices are $\left\langle {}^5D_0\right| U^{(J)} \left|{}^5F_2\right\rangle^2 = 0.00324$, $\left\langle {}^5D_0\right| U^{(J)} \left|{}^5F_4\right\rangle^2 = 0.00229$ and $\left\langle {}^5D_0\right| U^{(J)} \left|{}^5F_6\right\rangle^2 = 0.00023$ [44]. Since the rate of transition at each energy level is directly proportional to the integrated emission intensity, thus, the ratio of rate of electric dipole to magnetic dipole transition can be written as [45]

$$\frac{A_{0\to J=2,4,6}}{A_{0\to 1}} = \frac{I_{0\to J=2,4,6}}{I_{0\to 1}}\frac{h\nu_{0\to 1}}{h\nu_{0\to J=2,4,6}}. \tag{3}$$

Thus, with the help of equations (2) and (3), J–O parameter $\Omega_{J=2,4,6}$ can be calculated. In the present case, Ω_2 and Ω_4 are calculated but Ω_6 is not calculated because the emission of $^5D_0 \to {}^7F_6$ transition was not experimentally observed due to the instrumental limitations. Once the J–O parameter was calculated, other radiative parameters such as total transition probabilities (A_T), radiative lifetime decay (τ_{rad}) and radiative branching ratio (β_{rad}) were calculated using the relations given below. The total radiative transition probability can be obtained by the given relation [44–46]

$$A_{rad} = A_{ed} + A_{md} \tag{4}$$

and therefore

$$A_T(\psi J) = \sum\nolimits_{J'} A_{J\to J'}. \tag{5}$$

The radiative lifetime, τ_R of an excited level ΨJ is given by the reciprocal of the $A_T(\psi J)$ and can be written as

$$\tau_{rad}(\Psi J) = \frac{1}{\sum_{J'} A_{J\to J'}}. \tag{6}$$

Stronger emission probabilities and more transitions from a level lead to faster decay and shorter lifetimes.

The fluorescence branching ratio (β_{rad}) is another important radiative parameter used to understand the optical potentiality of the material

$$\beta_{rad}(\Psi J) = \frac{A(\Psi J, \Psi J')}{A_T(\Psi J)}. \tag{7}$$

Another radiative property named as the stimulated emission cross-section($\sigma(\lambda_p)$) can be expressed as

$$\sigma(\lambda_p)(J \to J') = \frac{\lambda_p^4}{8\pi c n^2 \Delta\lambda_{eff}} A_{rad}(J \to J'), \tag{8}$$

where λ_p is the wavelength of peak emission (in nm) and $\Delta\lambda_{eff}$ is the effective line width of the emission band found by dividing the area of the emission band by its maximum height.

The J–O parameter and other spectral parameters are summarized in table 2. It is generally accepted that Ω_2 is related to the covalence of rare earth bonds and it shows higher value when the ion occupies highly polarized and asymmetric sites. The Ω_4 and Ω_6 are related to the viscosity and rigidity of the host medium in which the ions are situated. The change in Ω_2 value with rare earth concentration indicates the change in the symmetric nature of Eu^{3+} in this host, which is also clearly indicated by the asymmetry ratio. The calculated value of β and ($\sigma(\lambda_p)$) are maximum for $^5D_0 \to {}^7F_2$ transition which is evident from the experimental results.

4. Conclusions

Eu^{3+}-doped ZnO/TiO_2 nanocomposite phosphors were successfully synthesized via low temperature co-precipitation route. The prepared sample is composed of both phases of hexagonal ZnO and tetragonal TiO_2. Due to mismatch of ionic radii of Eu^{3+} and Zn^{2+}/Ti^{4+} ions, a very slight shift in the main characteristic peaks of XRD pattern is observed which causes the decrease in the crystallite size. Apart from multi defect emissions, two very intense peaks around 594 and 619 nm were observed from the intra-4f transition of Eu^{3+} ions under the resonant excitation of 393 nm. Low temperature annealing is found more suitable for enhanced emission. Above 1.5 wt% Eu^{3+} quenching of photoemission occurs and 40 : 60 (ZnO : TiO_2) ratio is the most appropriate composition for getting maximum emission intensity. Higher value of the Judd–Ofelt parameter Ω_2 indicates higher covalence and more asymmetric environment around Eu^{3+} ions. The critical distance calculation and Dexter theory suggested that dipole–dipole interaction is responsible for concentration quenching. Optical band gap was calculated for different Eu and ZnO compositions and modification of band gap from 3.3 to 3.9 eV was observed. The strong red emission at 619 nm with better CIE chromaticity coordinates from pink to orange region make these phosphors suitable for potential optoelectronic and bio-related applications.

Acknowledgement

One of the authors, Baitha acknowledges ISM research scholars funding by Government of India. We are also grateful to Dr S. K. Sharma, Department of Applied Physics, ISM Dhanbad for PL and diffuse reflectance studies.

References

[1] Vijaya Kumar R, Maheshvaran K, Sudarsan V and Marimuthu K 2014 *J. Lumin.* **154** 160

[2] Astuti, Mikrajuddin Abdullah and Khairurrijal 2009 *Adv. Opt. Electron.* http://www.hindawi.com/journals/aoe/2009/918351

[3] Venkata Rao K, Babu S, Venkataiah G and Ratnakaram Y C 2015 *J. Mol. Struct.* **1094** 274

[4] Jie Yang, Bin Zhai, Xin Zhao, Zhiqiang Wang and Hai Lin 2013 *J. Phys. Chem. Solids* **74** 772

[5] Nikifor Rakov, Vieira S A, Silva Q P S and Maciel G S 2015 *Sensor. Actuat. B-Chem.* **209** 407

[6] Singh A K, Singh S K and Rai S B 2014 *RSC Adv.* **4** 27039

[7] Verma R K, Kumar K and Rai S B 2011 *J. Lumin.* **131** 988

[8] Pankaj Kr. Baitha and Manam J 2015 *J. Rare Earth* **33** 805

[9] Hom Nath Luitel, Kazuya Ikeue, Risa Okuda, Rumi Chand, Toshio Torikai, Mitsunori Yada and Takanori Watari 2014 *Opt. Mater.* **36** 591

[10] Wu Changle, Shen Li, Yong Cai Zhang and Qingli Huang 2012 *Mater. Lett.* **66** 83

[11] Akurati K K, Andri Vital, Jean-Philippe Dellemann, Katarzyna Michalow, Thomas Graule, Davide Ferri and Alfons Baiker 2008 *Appl. Catal. B-Environ.* **79** 53

[12] Shijun Liao, Huang Donggen, Denghua Yu, Yunlan Su and Gaoqing Yuan 2004 *J. Photoch. Photobio. B* **168** 7

[13] Kuzhalosai V, Subash B, Senthilraja A, Dhatshanamurthi P and Shanthi M 2013 *Spectrochim. Acta A* **115** 876

[14] Xiaochen Yu, Shaowei Liang, Zhongwang Sun, Yingwei Duan, Yanbin Qin, Li Duan *et al* 2014 *Opt. Commun.* **313** 90

[15] Ching-Ting Lee 2010 *Materials* **3** 2218

[16] Litty Irimpan, Bindu Krishnan, Nampoori V P N and Radhakrishnan P 2008 *Opt. Mater.* **31** 361

[17] Jungsik Bang, Heesun Yang and Holloway P H 2005 *J. Chem. Phys.* **123** 084709

[18] Sekhar H, Rakesh Kumar Y and Narayana Rao D 2015 *IOP Conf. Ser.: Mater. Sci. Eng.* **73** 012079

[19] Elias Burstin 1954 *Phys. Rev.* **93** 632

[20] Moss T S 1954 *Proc. Phys. Soc. Sect. B* **67** 775

[21] Escobedo Morales A, Sánchez Mora E and Pal U 2007 *Rev. Mex. Fis.* **53** 18

[22] Yasemin Caglar 2013 *J. Alloy Compd.* **560** 181

[23] Liu Huangqing, Wang Lingling, Chen Shuguang, Zou Bingsuo and Peng Zhiwei 2007 *Appl. Surf. Sci.* **253** 3872

[24] Mȧczka M, Fuentes A F, Hermanowicz K, Macalik L, Tomaszewski P E, Kępiński L and Lisiecki R 2010 *J. Nanosci. Nanotechnol.* **10** 5746

[25] Dieke G H 1968 *Spectra and energy levels of rare earth ions in crystals* (USA: Inter Science Publishers) pp 189–314 (SBN 470 21390 6)

[26] Bing Han, Pengju Li, Jingtao Zhang, Jie Zhang, Yongfei Xue, Xinying Suo *et al* 2015 *Mater. Lett.* **158** 208

[27] Li W, Frenkel A I, Woicik J C, Ni C and Ismat Shah S 2005 *Phys. Rev. B* **72** 155315

[28] Dutta S, Som S and Sharma S K 2013 *Dalton Trans.* **42** 9654

[29] Dexture D L 1953 *J. Chem. Phys.* **21** 836

[30] Ilhan M, Samur R, Demirer H and Mindivan F 2015 *Metalurgija* **54** 407

[31] Blasse G 1986 *J. Solid State Chem.* **62** 207

[32] Blasse G and Grabmarier B C 1994 *Luminescent materials* (Berlin: Springer-Verlag) p 99

[33] Yadav R S, Verma R K and Rai S B 2013 *J. Phys. D Appl. Phys.* **46** 275101

[34] Jan-Christoph Panitz, Jean-Claude Mayor, Beda Grob and Wilhelm Durisch 2000 *J. Alloy Compd.* **303–304** 340

[35] Repelin Y, Proust C, Husson E and Beny J M 1995 *J. Solid State Chem.* **118** 163

[36] Bin-Siang Tsai, Yen-Hwei Chang and Yu-Chung Chen 2005 *Electrochem. Solid St.* **8** H55

[37] Kuan-Wei Huang, Wei-Ting Chen, Cheng-I Chu, Shu-Fen Hu, Hwo-Shuenn Sheu, Bing-Ming Cheng *et al* 2012 *Chem. Mater.* **24** 2220

[38] Yu-Chun Li, Yen Hwei Chang, Yu-Feng Lin, Yee-Shin Chang and Yi-Jing Lin 2007 *J. Alloy Compd.* **439** 367

[39] Hunt R W G 1991 *Measuring colour: applied science and industrial technology* (New York: Ellis Horwood) 2nd ed

[40] Som S, Dutta S, Vijay Kumar, Vinod Kumar, Swart H C and Sharma S K 2014 *J. Lumin.* **146** 162

[41] Judd B R 1962 *Phys. Rev.* **127** 750

[42] Ofelt G S 1962 *J. Chem. Phys.* **37** 511

[43] Kumari P and Manam J 2016 *Spectrochim. Acta A* **152** 109

[44] Som S, Kunti A K, Vinod Kumar, Vijay Kumar, Dutta S, Chowdhury M *et al* 2014 *J. Appl. Phys.* **115** 193101

[45] Abhilash Kumar R G, Satoshi Hata and Gopchandran K G 2013 *Ceram. Int.* **39** 9125

[46] Swapna K, Mahamuda S K, Srinivasa Rao A, Sasikala T, Packiyaraj P, Rama Moorthy L and Vijay Prakash G 2014 *J. Lumin.* **156** 80